AIAA JOURNAL
Vol. 38, No. 2, February 2000

Large Eddy Simulation of Aircraft Wake Vortices Within Homogeneous Turbulence: Crow Instability

Jongil Han,* Yuh-Lang Lin,† David G. Schowalter,‡ and S. Pal Arya§
North Carolina State University, Raleigh, North Carolina 27695-8208
and
Fred H. Proctor¶
NASA Langley Research Center, Hampton, Virginia 23681

Ambient atmospheric turbulence effects on aircraft wake vortices are studied using a validated large eddy simulation model. Our results confirm that the most amplified wavelength of the Crow instability and the lifetime of wake vortices are significantly influenced by ambient turbulence (Crow, S. C., "Stability Theory for a Pair of Trailing Vortices," *AIAA Journal*, Vol. 8, No. 12, 1970, pp. 2172–2179). The Crow instability becomes well developed in most atmospheric turbulence levels, but in strong turbulence the vortex pair deforms more irregularly due to turbulence advection. The most amplified wavelength of the instability decreases with increasing dimensionless turbulence intensity η, although it increases with increasing turbulence integral length scale. The vortex lifespan is controlled primarily by η and decreases with increasing η, whereas the effect of integral scale of turbulence on vortex lifespan is of minor importance. The lifespan is estimated to be about 40% larger than Crow and Bate's predicted value (Crow, S. C., and Bate, E. R., "Lifespan of Trailing Vortices on a Turbulent Atmosphere," *Journal of Aircraft*, Vol. 13, No. 7, 1976, pp. 476–482) but in agreement with Sarpkaya's recent modification (Sarpkaya, T., "Decay of Wake Vortices of Large Aircraft," *AIAA Journal*, Vol. 36, No. 9, 1998, pp. 1671–1679) to Crow and Bate's theory. This larger lifespan is also supported by data from water tank experiments and direct numerical simulations. There appears to be a possibility that the scatter in vortex lifespans due to ambient turbulence alone decreases with increasing Reynolds number, whereas larger scatter of lifespans in flight tests may result from other factors such as stratification, wind shear, and inhomogeneous ambient turbulence.

I. Introduction

EXISTING procedures for aircraft separations prevent unsafe encounters with hazardous wake vortices but are independent of ambient meteorology and can impact airport capacity. The development of a forecasting system that includes atmospheric variables can be useful for reducing aircraft separations, maintaining safety, and benefiting airport capacity. NASA is developing an automated system, called the Aircraft Vortex Spacing System (AVOSS),[1,2] that will determine safe operating spacing between arriving and departing aircraft as based on the observed or predicted weather conditions. To develop this system, research is being focused on understanding how wake vortices interact with the atmosphere. In the present work we focus on the effects of ambient atmospheric turbulence on the Crow instability[3] as well as vortex lifespan using a validated numerical model. Results from this work and parallel efforts are to provide support in the development of the AVOSS system.

Crow instability is an important mechanism that eventually brings about the destruction of wake vortices.[3] This instability is based on linear theory and was first analyzed in terms of mutual induction by Crow. Because of the Crow instability, the vortices undergo a symmetric and sinusoidal instability that grows exponentially and, finally, result in a linking into a series of crude vortex rings. This phenomenon has been observed by flight tests[4,5] and laboratory experiments,[6–8] as well as confirmed in numerical simulations.[9,10]

During development of the Crow instability, the vortex behavior is significantly influenced by atmospheric turbulence, stratification and wind shear, and vortex core bursting, which are believed to be main causes of deviations from the predictions of the instability theory on the most amplified wavelength and vortex lifespan. Core bursting,[7,11] which falls outside the scope of the present study, is another dominant instability mechanism for vortex destruction, but it more often occurs toward the end of the vortex lifespan.

Turbulence, whose scale is smaller than vortex separation distance, can lead to an enhanced diffusion of the circulation of the vortices,[12–14] whereas strong and large turbulent eddy motion can cause a large distortion of the vortices.[5,10] The enhancement of vortex decay due to ambient turbulence is one important factor of the wake-prediction models developed by Donaldson and Bilanin[12] and Greene[13] and will be studied in more detail in a separate paper. On the other hand, the vortices may distort the ambient turbulence and cause departures from statistical homogeneity and isotropy. This nonlinear interaction between the vortices and the ambient turbulence may modify the predictions from the linear instability theory.

Crow and Bate[15] (CB) incorporate the effects of ambient turbulence to the Crow instability and then obtain the theoretical predictions for the vortex lifespan. They define the vortex lifespan as the time at which linking of a vortex pair occurs. Under the assumption that eddies of the relevant size lie in the Kolmogorov inertial subrange that is characterized by the turbulence energy dissipation rate ϵ and that the atmospheric turbulence is independent of the vortices, they predict that the dimensionless vortex lifespan,

$$\tau = (\Gamma_0/2\pi b_0^2)t^* \tag{1}$$

is only a function of the dimensionless turbulence intensity η:

$$\eta = (\epsilon b_0)^{\frac{1}{3}}/V_0, \qquad V_0 = \Gamma_0/2\pi b_0 \tag{2}$$

where Γ_0 is the circulation around the vortices, t^* is the vortex lifespan, and b_0 is the initial separation distance of the vortex pair. Here, η represents the ratio of the characteristic turbulent velocity scale at the scale of the vortex separation distance $[(\epsilon b_0)^{1/3}]$ to the speed of descent of the vortex pair by mutual induction, V_0, and is the appropriate dimensionless measure of turbulence intensity. The theoretical prediction function $\tau(\eta)$ appears to be in reasonable

Received 16 March 1998; revision received 20 October 1998; accepted for publication 17 June 1999. This material is declared a work of the U.S. Government and is not subject to copyright protection in the United States.

*Researcher, Department of Marine, Earth and Atmospheric Sciences.
†Professor, Department of Marine, Earth and Atmospheric Sciences; yl_lin@ncsu.edu.
‡Visiting Assistant Professor, Department of Marine, Earth and Atmospheric Sciences; currently Aerospace Industry Team Engineer, Fluent Inc., Lebanon, NH 03766.
§Professor, Department of Marine, Earth and Atmospheric Sciences.
¶Research Scientist, Flight Dynamics and Control Division. AIAA Member.

agreement with data from field flight tests, but the scatter is large (about a factor of 3 in τ for fixed η), which may be due to other influences such as wind shear, stratification, and core bursting, as mentioned earlier.

On the other hand, from dimensional arguments, Sarpkaya and Daly[7] postulated a similarity relation

$$H = h/b_0 = f(T, \eta, L_{11}/b_0) \tag{3}$$

in the absence of wind shear and stratification, where h is the descent distance of the vortices, T is dimensionless time, that is,

$$T = V_0 t/b_0 \tag{4}$$

and L_{11} is the longitudinal integral length scale in the axial direction of a vortex, defined as

$$L_{11} = \int_0^\infty \langle u(x)u(x+r)\rangle \Big/ \langle u^2\rangle \, dr \tag{5}$$

where $\langle\ \rangle$ is the domain average. Then, in the water tank experiments in which two biplanar grids were towed at a constant speed to produce isotropic turbulence, they found that the descent and demise of the vortices are controlled primarily by the dissipation rate of ambient turbulence, whereas the integral scale of turbulence plays only a minor role. Compared with flight tests, the water tank data displayed less scatter because the effects of ambient wind shear and stratification were avoided. Liu[8] performed similar experiments in a towing water tank. His results showed that, when the lifespan only due to vortex linking is considered, the scatter in lifespans is much less and that the dominant wavelength of the linking decreases with increasing turbulence intensity or dissipation rate.

The direct numerical simulation (DNS) results by Spalart and Wray,[10] in which a five by five array of vortex pairs is simulated in an initially isotropic turbulence without ambient wind shear and stratification, show a large scatter comparable with flight tests for the theoretical curve of CB. Because their DNS study showed no core bursting (to date, no numerical simulations of wake vortices have shown this phenomenon), the large scatter in their DNS results could be due to the variability of turbulence related to low Reynolds number flow characteristics intrinsic in any DNS study.

One way to investigate high-Reynolds-number flows, such as atmospheric boundary-layer turbulence, is through the use of a large eddy simulation (LES) model, which has become a useful tool for the study of interior turbulence structure.[16–18] In LES, the large-scale eddies are explicitly resolved, whereas small-scale eddies are parameterized through a closure model. One reason for the success of this approach is that the small-scale eddies tend to be more isotropic and universally similar and are, therefore, more amenable to parameterization than the large-scale eddies, which are much more dependent on the type of flow. The basic requirement of LES is that the grid size should be much smaller than the integral length scale to guarantee the isotropy of the subgrid-scale eddies. The numerical model used in the present study is a three-dimensional, nonlinear, compressible, nonhydrostatic LES model, namely, the Terminal Area Simulation System (TASS),[19,20] that has been adapted for simulation of interaction of wake vortices with the atmosphere.[20,21] We simulated only the post-rollup wake vortices; the rollup process falls outside the scope of the present study.

In Sec. II we describe our LES model and the modifications required for initial conditions. In Sec. III we present results from systematic numerical experiments in terms of dimensionless turbulence intensity and length scale. Finally, in Sec. IV we summarize our LES results and draw some conclusions.

II. Model and Initial Conditions

A. Model

The TASS model contains 12 prognostic equations: three for momentum, one each for pressure deviation and potential temperature, six coupled equations for continuity of water substance (water vapor, cloud droplet, cloud ice crystals, rain, snow, and hail), and one for a massless tracer (see Refs. 19 and 20 by Proctor for the whole TASS equation set). In the neutral and dry atmosphere neglecting the Coriolis force, the model equations can be reduced to four prognostic equations given by

$$\frac{\partial u_i}{\partial t} + \frac{1}{\rho_0}\frac{\partial p}{\partial x_i} = -\frac{\partial u_i u_j}{\partial x_j} + u_i\frac{\partial u_j}{\partial x_j} + \frac{1}{\rho_0}\frac{\partial \tau_{ij}}{\partial x_j} + \boldsymbol{f} \tag{6}$$

$$\frac{\partial p}{\partial t} + \frac{C_p P_0}{C_v}\frac{\partial u_j}{\partial x_j} = 0 \tag{7}$$

where u_i is the component of velocity, t is time, p is deviation from the reference atmospheric pressure P_0, ρ_0 is the reference air density, C_p and C_v are the specific heats of air at constant pressure and volume, and $\boldsymbol{f}$ is an artificial external forcing term to generate an isotropic turbulence. The equation for pressure deviation [Eq. (7)] has been derived from the mass continuity equation,[19] with the advection and subgrid eddy transport terms for pressure neglected in this study because of the dominance of the second term on the left-hand side of Eq. (7).

The dependent variables in TASS are treated as averages over the grid volumes, giving rise to subgrid stress terms. The subgrid stress τ_{ij} is approximated by using Smagorinsky first-order closure:

$$\tau_{ij} = \rho_0 K_m D_{ij} \tag{8}$$

where the velocity deformation D_{ij} is defined as

$$D_{ij} = \frac{\partial u_i}{\partial x_j} + \frac{\partial u_j}{\partial x_i} - \frac{2}{3}\frac{\partial u_k}{\partial x_k}\delta_{ij} \tag{9}$$

and the subgrid eddy viscosity is given by

$$K_m = (c_s\Delta)^2|Def| \tag{10}$$

The subgrid length scale Δ is constant and related to the grid size as $\Delta = (2\Delta x 2\Delta y 2\Delta z)^{1/3}$, $|Def| = \sqrt{(\frac{1}{2}D_{ij}\cdot D_{ij})}$. The coeffcient $c_s = 0.075$ was used as the optimum value; this value was found to be large enough to damp out small-scale fluctuations but small enough to avoid too much damping of the turbulence energy in higher wave numbers.

The TASS model uses the time-splitting integration procedure (small time step for acoustically active terms and large time step for advection and diffusion[22]) that results in a substantial savings in computing time. Local time derivatives (both small and large time steps) are approximated by the second order Adams–Bashforth method. Space derivatives are approximated by central differences in quadratic-conservative form, which are fourth order for advective derivatives and second order for remaining derivatives. Details of the numerical formulation can be found in Refs. 19 and 20. The numerical schemes used in TASS produce accurate and stable results and have been shown to have almost no numerical dissipation.[23]

The vortex system is representative of the post-rollup wake velocity field and is initialized with the superposition of two counter-rotating vortices, with the velocity field for each vortex specified as[24,25]

$$V(r) = \Gamma_0/2\pi\left[r/(r_c^2 + r^2)\right] \tag{11}$$

where $V(r)$ is the vortex tangential velocity at radius r; r_c is the core radius, that is, radius of peak tangential velocity; and Γ_0 is the circulation at $r \gg r_c$. In this study r_c is fixed as 2 m.

Grid points used in our simulations are $324 \times 112 \times 112$ with grid size $(\Delta x, \Delta y, \Delta z) = (1.0, 0.75, 0.75$ m), where x, y, and z correspond to the axial, lateral, and vertical directions of the vortex system and corresponding velocity components are u, v, and w, respectively. Periodic boundary conditions are imposed at all domain boundaries. Two values of b_0, that is, $b_0 = 16$ and 8 m, are used for fixed-domain size. For the case of $b_0 = 16$ m, the domain size becomes $(L_x \times L_y \times L_z) = (20b_0 \times 5b_0 \times 5b_0)$. The domain size in the axial direction, $20b_0$, is large enough to simulate the most amplified wavelength of about $8.6b_0$ for Crow instability.[3] The domain size of $5b_0$ in the lateral and vertical directions is sufficiently large to minimize boundary influences. The strain rate of neighboring vortex pairs that are present outside of the domain when periodic boundary conditions are assumed is only a few percent of that exerted by one

vortex on the other in the vortex pair. This domain configuration is adequate, although a larger domain size would be preferable if not limited by computing resources. For the case of $b_0 = 8$ m, the domain size becomes much larger in terms of b_0. The core size 2 m used in our simulations is larger than the typical value (about 5% of the generating aircraft's wingspan[20]) observed behind aircraft. However, dependency of r_c/b_0 on the Crow instability is weak[3] and is examined further when our LES results are compared with the theoretical predictions in Sec. III.

B. Initial Conditions

Because we want to study the effect of ambient turbulence on the Crow instability,[3] it is of crucial importance to obtain an initially homogeneous and isotropic turbulence field. Toward this purpose, the initial turbulence field is allowed to develop under an artificial external forcing at low wave numbers.[26] Because the TASS code uses a finite difference numerical scheme, the forcing is achieved by performing, first, a three-dimensional fast Fourier transform (FFT) at every large time step, then adding a constant amplitude f to all of the modes with integer wave numbers whose magnitude is less than 3.0, and, finally, performing an inverse FFT back to the physical space. The wave number in the axial direction is normalized so that the axial wavelength has the same magnitude as that of the corresponding wave number in the lateral or the vertical direction. Because of viscous dissipation, the simulation can reach a statistically steady state in the sense that the mean turbulence kinetic energy (TKE) oscillates in time around a constant value. Figure 1 shows that the domain-averaged TKE and variances from resolved velocity fields reach a steady state around about 1000 s. The integral length scale is calculated as $L_{11} = 15.0$ m in a steady-state turbulence, and the large eddy turnover time, defined as

$$t_e = L_{11}/\langle u^2\rangle^{\frac{1}{2}} \tag{12}$$

is estimated as $t_e = 56.2$ s. Thus, we obtain a statistically steady-state flow after integration over about 18 large eddy turnover times. The isotropy parameter I, defined as

$$I_1 = [\langle u^2\rangle/\langle v^2\rangle]^{\frac{1}{2}} \quad \text{or} \quad I_2 = [\langle w^2\rangle/\langle v^2\rangle]^{\frac{1}{2}} \tag{13}$$

fluctuates only a few percent around its expected value of 1 for isotropic turbulence. Therefore, our simulated turbulence is close to statistical isotropy.

Figure 2 shows the one-dimensional spectra of u and v in the statistically steady state as functions of wave number κ_1, where subscript 1 represents axial direction. Fairly extensive inertial subranges with

$$F_{11}(\kappa_1)\kappa_1^{\frac{5}{3}}\langle\epsilon\rangle^{-\frac{2}{3}} = \alpha_1 \tag{14}$$

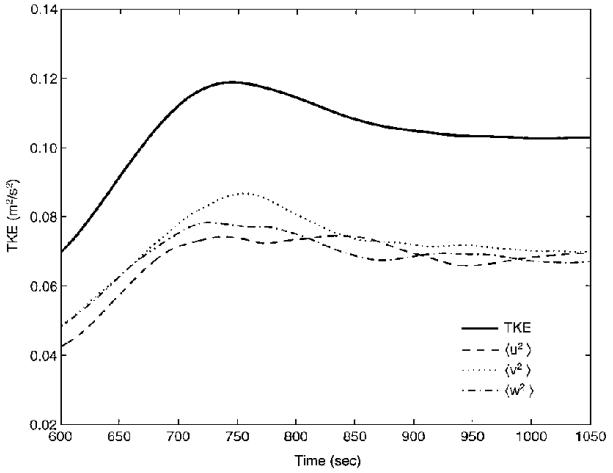

Fig. 1 Time evolution of turbulent kinetic energy and velocity variances before vortex injection.

Table 1 Characteristics of the numerical simulations

Turbulence strength	η	b_0, m	r_c, m	Domain size ($L_x \times L_y \times L_z$)
Weak	0.0316	16	2	$20b_0 \times 5b_0 \times 5b_0$
		8	2	$40b_0 \times 10b_0 \times 10b_0$
	0.0789	16	2	$20b_0 \times 5b_0 \times 5b_0$
Moderate	0.1753	16	2	$20b_0 \times 5b_0 \times 5b_0$
		8	2	$40b_0 \times 10b_0 \times 10b_0$
Strong	0.3506	16	2	$20b_0 \times 5b_0 \times 5b_0$
		8	2	$40b_0 \times 10b_0 \times 10b_0$
	0.5844	16	2	$20b_0 \times 5b_0 \times 5b_0$

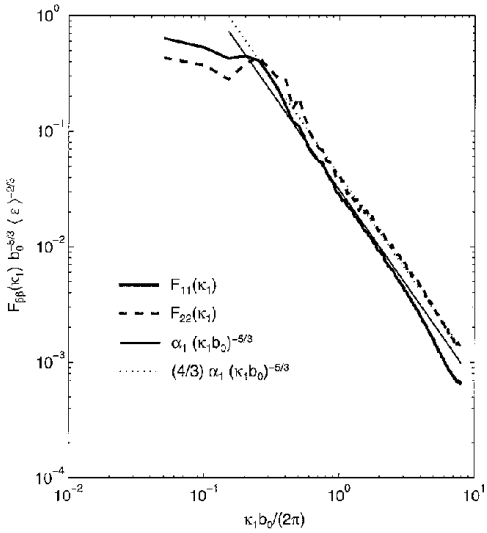

Fig. 2 One-dimensional energy spectrum in a steady-state turbulence before vortex injection.

$$F_{22}(\kappa_1)\kappa_1^{\frac{5}{3}}\langle\epsilon\rangle^{-\frac{2}{3}} = \tfrac{4}{3}\alpha_1 \tag{15}$$

are present, where $F_{11}(\kappa_1)$ and $F_{22}(\kappa_1)$ are one-dimensional longitudinal and transverse spectra, respectively, $\langle\epsilon\rangle$ represents a domain-averaged TKE dissipation rate, and α_1 is a constant. If the Kolmogorov constant α is taken as 1.5 (e.g., see Ref. 27), then we can estimate $\langle\epsilon\rangle$ from a line fit of the theoretical relations of the spectra in the inertial subrange, that is, Eqs. (14) and (15) with $\alpha_1 = (\frac{18}{55})\alpha$, to the simulated spectra, as seen in Fig. 2. For our simulated turbulence field, the dissipation rate is calculated as $\langle\epsilon\rangle \approx 0.9897 \times 10^{-3}$ m^2 s^{-3}.

A two-dimensional counter-rotating vortex pair prescribed by Eq. (11) is initialized in every y–z plane along the axial direction when the ambient turbulence reaches a steady state, that is, at 1020 s after integration. Five values for η are obtained by varying the circulation to save computing time, rather than by varying $\langle\epsilon\rangle$, and can be divided into three turbulence strength groups, as seen in Table 1. The vortex injection time is the same for each η value unless stated otherwise.

Except in one case, that is, the case of $\eta \approx 0.0$ described in Sec. III, the flow is turbulent with Reynolds numbers ($Re \equiv \Gamma/\nu$, where ν is kinematic viscosity) ranging from 2.88×10^6 to 5.33×10^7, which are appropriate for atmospheric wake vortices.

III. Results

A. Crow Instability

Figure 3 shows top and side views of the vortex pairs with increasing nondimensional time for six different nondimensional turbulence intensities. In the case of $\eta \approx 0.0$ (Fig. 3a), a constant viscosity is used for the subgrid stress ($Re \approx 1.66 \times 10^4$) and the instability is initiated by adding very small random velocity perturbations to the initial field. This case is representative of nearly laminar flow and is useful for comparing with the cases that have turbulence. The method of Jeong and Hussain[28] is used for the identification

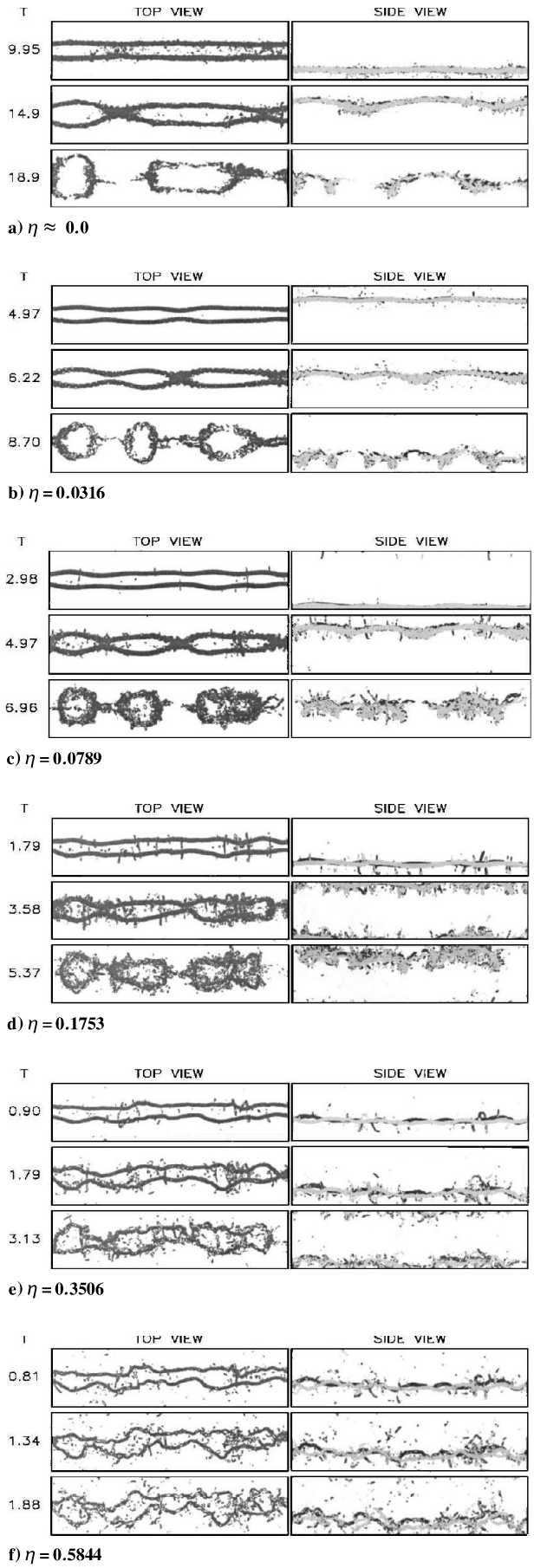

Fig. 3 Top (x, y) and side (x, z) views of wake vortices at three nondimensional times for the case of $b_0 = 16$ m.

of a vortex. They define a vortex in terms of the second negative eigenvalue λ_2 of the symmetric tensor $\boldsymbol{S}^2 + \Omega^2$, where $\boldsymbol{S}$ and Ω are, respectively, the symmetric and antisymmetric parts of the velocity gradient tensor $\nabla \boldsymbol{u}$. Corjon et al.[29] applied this method for the identification of wake vortices and showed that an isosurface of negative λ_2 visualizes the vortices very well. In the present study, the top (side) view is taken from the x–y (x–z) plane projection of the minimum negative λ_2 value along the $z(y)$ direction. A threshold λ_2 value to identify the vortex is arbitrarily determined. In the TASS code the vortex center position to estimate the most amplified wavelength is later calculated via the centroid of $\zeta_x \times p^6$, where ζ_x and p represent axial vorticity and pressure perturbation, respectively.

Except for strong turbulence, most of the cases in Fig. 3 show clearly developing Crow instability. In agreement with observations, the vortex pair connects together as a result of the instability, forms a train of vortex rings, and then disintegrates into a turbulent state. In strong turbulence, the vortices are more irregularly distorted due to advection and nonlinear interaction with ambient turbulence. A sinusoidal instability still appears to develop even for a strong turbulence cases. This vortex behavior for strong turbulence was observed by Tombach[5] (e.g., see Fig. 4 in Ref. 5). Spalart and Wray's[10] DNS study also shows similar patterns, but their results for intense turbulence appear to be dominated by ambient turbulent flow advection without the indication of the sinusoidal development of Crow instability.[3]

The dimensionless vortex linking time, defining the vortex lifespan, decreases with increasing nondimensional turbulence intensity, which is consistent with previous studies.[5,7,8,10,15] Vortex lifespan will be discussed in detail later. Note that the vortex linking time for the case of $\eta \approx 0.0$ (Fig. 3a) is much larger than for cases with ambient turbulence (Figs. 3b–3f). The significant λ_2 values around the vortex pair may result from the stretching of the ambient turbulent eddies in the vertical direction by the velocity field induced by the vortices, as suggested in the Corjon et al.'s[29] DNS study. The circulation associated with the vortices can be weakened through this turbulence vorticity stretching process. The issues involving vortex decay will be discussed in a separate paper.

In the top views of Fig. 3, the most amplified wavelength (MAW) appears to decrease with increasing turbulence intensity. A quantitative estimate of the MAW can be obtained from the spectrum analysis of y displacement of the vortex along the axial direction just before vortex linking (Fig. 4). The MAWs for $\eta = 0.0316$, 0.0789, and 0.1753 range from $4b_0$ to $7b_0$, showing higher value for weaker turbulence. For stronger turbulence, that is, $\eta = 0.3506$ and 0.5844, a significant spectral energy of the displacement is seen in the smaller wavelength range. The case of $\eta \approx 0.0$ shows the largest MAW, that is, about $10b_0$. This trend that the MAW decreases with increasing turbulence intensity agrees surprisingly well with results of Liu's[8] laboratory experiments. It is noticeable that stronger turbulence tends to intensify more strongly smaller unstable wavelengths than larger ones.

According to Crow's linear instability theory,[3] both the MAW and the amplification rate depend only on r_c/b_0, though the dependency is weak. Crow obtained the MAW of $8.6b_0$ with $r_c/b_0 = 0.0985$, assuming that $d/(2r_c) = 0.321$ for vortices trailing from an elliptically loaded wing and that vorticity is uniformly distributed within the vortex core. Here, d is the cutoff distance in the line integral representing self-induction. Because a value of $r_c/b_0 = 0.125$ is used in our simulations, the MAW predicted by Crow's theory is about $8.2b_0$, which is larger than any MAW obtained in our simulations with ambient turbulence. In laboratory experiments, Liu[8] obtained an average MAW of $7.8b_0$, whereas Spalart and Wray's[10] DNS results show an average MAW of $6.7b_0$. In Chevalier's[4] flight tests, the MAWs range from $5b_0$ to $10b_0$ in light atmospheric turbulence conditions, showing a large scatter about the average value of $8.4b_0$. A close inspection of his observations indicates that the MAW tends to decrease with increasing air speed. Because the circulation of the vortices is inversely proportional to the air speed [i.e., $\Gamma_0 = 4Mg/(\pi\rho V_a B)$, where B is the span of the generating aircraft, V_a is the air speed, and M is the mass of the generating aircraft], η becomes large as air speed increases. Thus, the observations by Chevalier indicate that, assuming the ambient turbulence intensity did not change much during the flight tests, the MAW tends

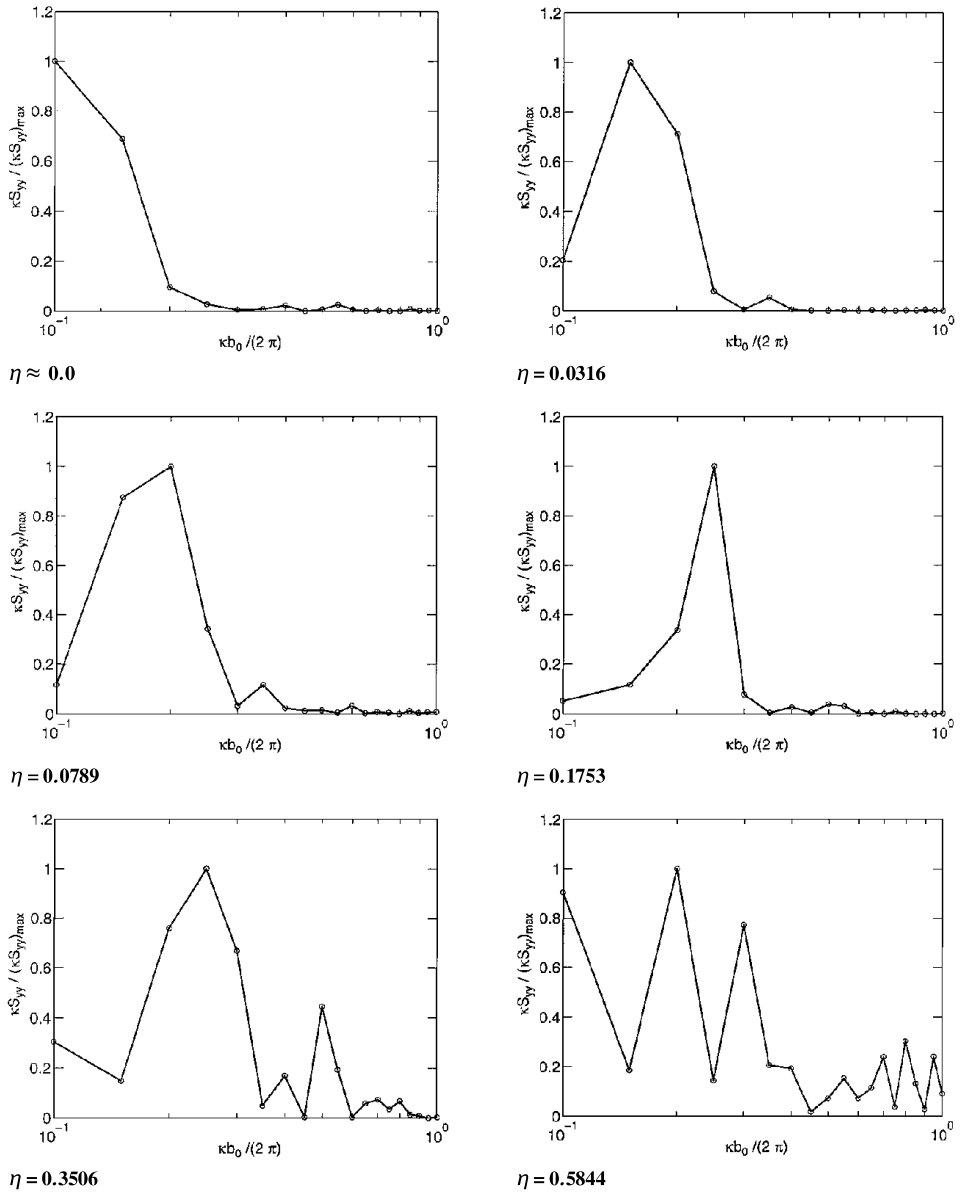

Fig. 4 Spectrum of y displacement of the vortex along the axial direction before vortex linking for the case of $b_0 = 16$ m.

to decrease with increasing nondimensional turbulence intensity, which is consistent with our results. However, the measurement errors and the absence of the turbulence dissipation rate measurement make it difficult to compare closely our results with those observations.

The smaller MAW compared with Crow's[3] linear theory in the case of $b_0 = 16$ m may come from the limited domain size used in the present study or the artificial external forcing added in a wavelength range of $1.7b_0$–$5b_0$ to maintain the ambient turbulence intensity. Another possibility is the difference of the vortex model used in the two studies; for example, unlike the Crow case, the vorticity within the vortex core in the present study decreases with increasing radial distance from the vortex center. Finally, the effect of the ambient turbulence length scale on the vortices must be considered. Although not shown in the figures, our previous test results have indicated that the artificial external forcing and the difference of the vortex model used are not relevant to the discrepancy between the Crow theory and the present results. For example, although the external forcing was deactivated at vortex injection time so that the ambient turbulence strength decreased with time, the instability development was almost identical to that with the external forcing, confirming the arguments by Corjon et al.[29] that the timescale of the ambient turbulence compared to that of the vortex is sufficiently large to obtain the main characteristics of the effects of ambient turbulence on the wake vortices. We have also tested the instability development for the Rankine vortex model. The Rankine vortex model possessing uniform vorticity distribution within the vortex core is exactly the same that used in Crow's theory.[3] The instability development for the Rankine vortex model was also almost the same as that of the present model, indicating that the instability is very sensitive neither to the vortex model used nor to its core structure.

The much larger value of the MAW, that is, about $10b_0$, in the case of $\eta \approx 0.0$ indicates that our domain size is large enough to produce the Crow instability.[3] However, the problem for the limited domain size results because the scales of the ambient turbulence are limited by the domain size. Note that the Crow MAW, that is, $8.2b_0$ for $r_c/b_0 = 0.125$, is not within the inertial subrange (Fig. 2) but larger than the domain in the y–z plane. Therefore, some sensitivity tests with $b_0 = 8$ m for $\eta = 0.0316$, 0.1753, and 0.3506 were conducted to see the effect of ambient turbulence length scale on the instability. In terms of vortex separation distance, the domain size in this case is enlarged to $(L_x \times L_y \times L_z) = (40b_0 \times 10b_0 \times 10b_0)$, that is, just twice of the case of $b_0 = 16$ m in each direction (Table 1). The integral length scale of the ambient turbulence also becomes about

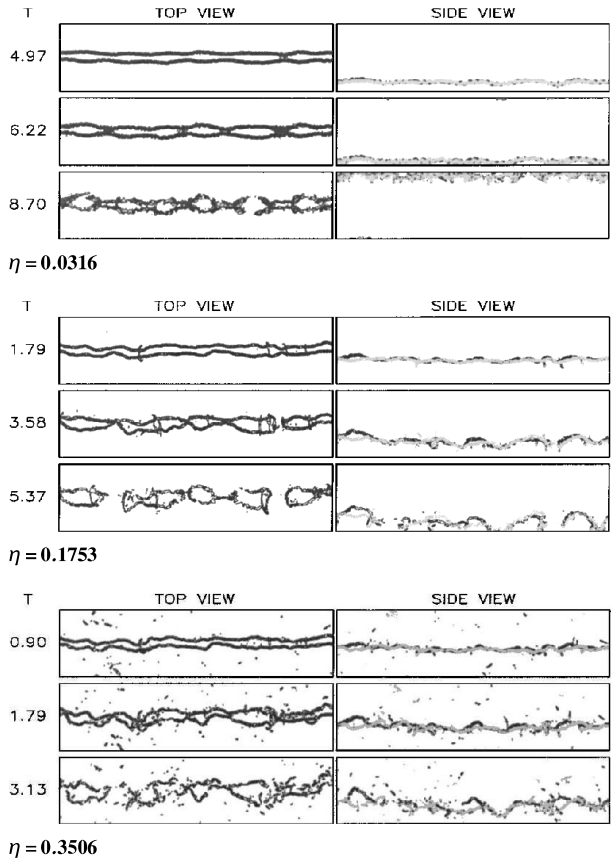

Fig. 5 Top (x, y) and side (x, z) views of wake vortices at three nondimensional times for the case of $b_0 = 8$ m.

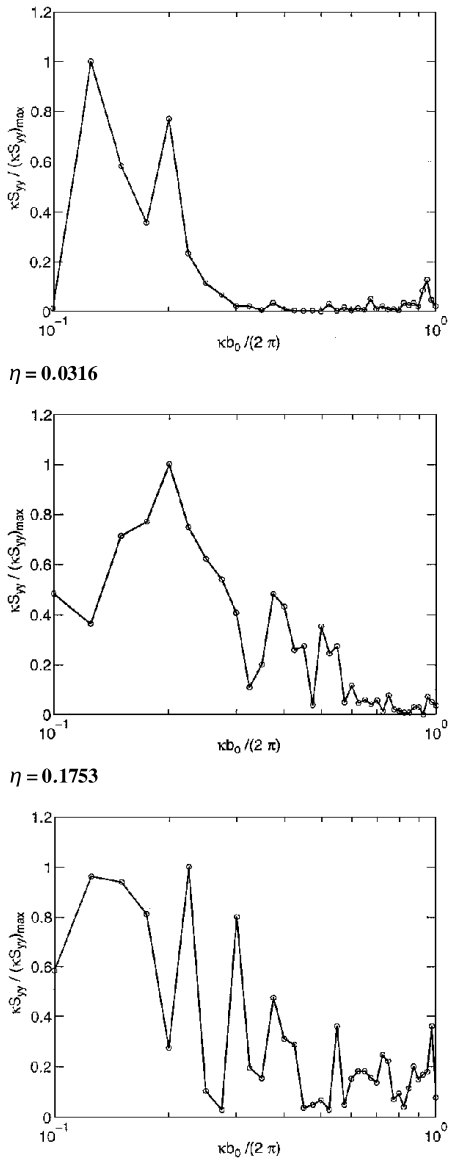

Fig. 6 Spectrum of y displacement of the vortex along the axial direction before vortex linking for the case of $b_0 = 8$ m.

twice the vortex separation distance. The MAW for the Crow instability based on the theory is estimated to be $6.9b_0$, which is quite well located in the middle of the inertial subrange of Fig. 2. (In this case the values on κ_1 axis of Fig. 2 should be divided by 2.) The top and side views and the y-displacement spectra for the larger integral length scale of turbulence are shown in Figs. 5 and 6, respectively. Because domain size in the axial direction is doubled, more vortex rings are formed (Fig. 5) compared with the case of $b_0 = 16$ m (Fig. 3). The vortex evolution appears to be similar to the previous case, but the MAW is a little larger, for example, the spectral peaks of y displacements for $\eta = 0.0316$ and 0.1753 are $8b_0$ and $5b_0$ compared to $7b_0$ and $4b_0$ in the preceding case, respectively. Although not shown in Fig. 6, the strongest spectral peaks of y displacements for $\eta = 0.1753$ and $\eta = 0.3506$ are at $20b_0$, which may reflect the advection effect due to larger turbulent eddy motions but is not directly related to instability. Considering the theoretical MAWs in the cases of both $b_0 = 16$ and 8 m, that is, $8.2b_0$ and $6.9b_0$, respectively, the MAW in the case of $b_0 = 8$ m is relatively larger than that in the case of $b_0 = 16$ m. Therefore, larger scales of ambient turbulence tend to promote larger MAW. In addition, for the case of $b_0 = 8$ m, the theoretical MAW can be produced within our dimensionless turbulence strength range, especially in the weak turbulence case. The results with larger turbulence integral length scale are more consistent with Chevalier's[4] atmospheric observations and Liu's[8] laboratory experiments in that all include the theoretical MAW within the obtained MAW range.

B. Vortex Lifetime

In this study, following CB's definition,[15] the vortex lifetime or lifespan is defined as the time at which linking of a vortex pair occurs. Using Crow's original theory,[3] CB developed a composite vortex lifespan function by considering the cases of both very strong and very weak turbulence.[15] Their expression for vortex lifespan was based on the assumptions that the ambient atmospheric turbulence is independent of the vortices and that turbulent eddies of size comparable to the MAW lie in the Kolmogorov inertial subrange. According to CB, the vortex lifespan in strong turbulence is given by

$$t = \left[\frac{55}{81\Gamma(\frac{1}{3})\alpha}\right]^{\frac{1}{2}} \frac{b_0}{(\epsilon b_0)^{\frac{1}{3}}} \tag{16}$$

In dimensionless form with the Kolmogorov constant $\alpha = 1.5$,

$$\tau = 0.41/\eta \tag{17}$$

CB also obtained an equation for vortex lifespan in weak turbulence as

$$b_0^2 = \frac{24}{55} \frac{\alpha\epsilon^{\frac{2}{3}}\kappa_m^{-\frac{5}{3}} e^{2a(\kappa_m)t}}{[a(\kappa_m)\tan\theta(\kappa_m)]^2} \left[\frac{\pi}{|a''(\kappa_m)|t}\right]^{\frac{1}{2}} \tag{18}$$

where κ_m is the wave number of the MAW mode, a is the rate of displacement amplification, and θ is the angle of the vortex displacement from the horizontal plane. From the Crow theory,[3] $\kappa_m = 0.73/b_0$, $a(\kappa_m) = 0.83(\Gamma/2\pi b_0^2)$, $\tan\theta(\kappa_m) = 1.11$, and $|a''(\kappa_m)| = 3.12(\Gamma/2\pi)$. The $a''(\kappa_m)$ was evaluated from parabolic fit to the amplification rate curve for $r_c/b_0 = 0.0985$. Finally, the vortex lifespan

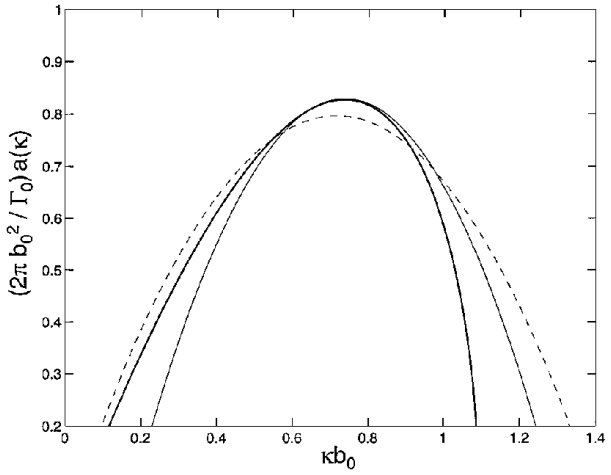

Fig. 7a Dimensionless amplification curve and its parabolic fit: ——, theoretical dimensionless amplication curve by Crow[3] for $r_c/b_0 = 0.0985$; ——, a parabolic fit to the amplification curve in present study; and - - -, a parabolic fit to the amplification curve used by CB.[15]

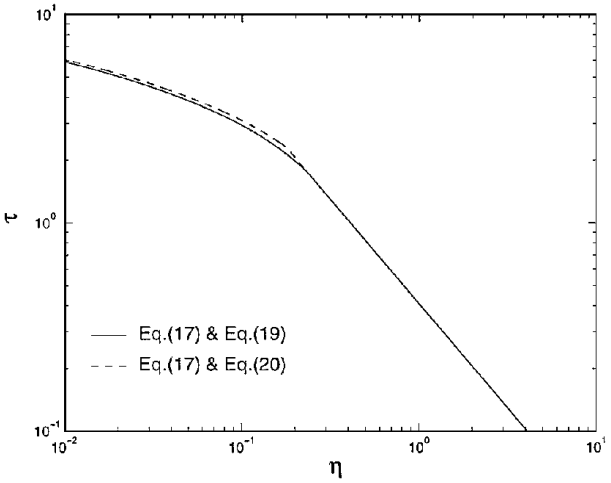

Fig. 7b Composite dimensionless lifespans according to the formula for strong turbulence [Eq. (17)] and for weak turbulence [Eqs. (19) and (20)].

expression obtained by CB[15] for weak turbulence in dimensionless form becomes

$$\eta = 0.87\tau^{\frac{1}{4}}e^{-0.83\tau} \tag{19}$$

We reevaluate $a''(\kappa_m)$ and find that the approximate coeffcient is about 4.90 instead of 3.12 from a parabolic fit to the amplification rate curve, as shown in Fig. 7a. With this refined value, the vortex lifespan for weak turbulence is

$$\eta = 0.98\tau^{\frac{1}{4}}e^{-0.83\tau} \tag{20}$$

Figure 7b shows that the new expression gives a larger lifespan for given η than the original one, but the difference between Eq. (19) and (20) is rather small. For example, the dimensionless lifespan from Eq. (20) at $\eta = 0.1$ is only about 5% larger than that of the lifespan from Eq. (19).

The vortex lifespan expression for the cases of $b_0 = 16$ and 8 m with a fixed $r_c = 2$ m is obtained following the method of CB[15] to compare with our LES results. It is estimated that, for the case of $b_0 = 16$ m, $\kappa_m = 0.77/b_0$, $a(\kappa_m) = 0.82(\Gamma/2\pi b_0^2)$, $\tan\theta(\kappa_m) = 1.10$, and $|a''(\kappa_m)| = 4.3(\Gamma/2\pi)$, whereas for the case of $b_0 = 8$ m, $\kappa_m = 0.91/b_0$, $a(\kappa_m) = 0.80(\Gamma/2\pi b_0^2)$, $\tan\theta(\kappa_m) = 1.10$, and $|a''(\kappa_m)| = 2.54(\Gamma/2\pi)$. Thus, with $\alpha = 1.5$, the vortex lifespan

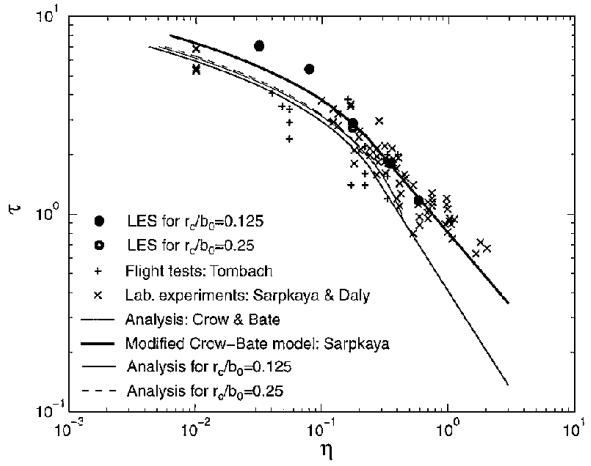

Fig. 8 Dimensionless vortex lifespans from numerical simulations, laboratory experiments, and flight tests.

for weak turbulence when $b_0 = 16$ m is approximated by

$$\eta = 0.97\tau^{\frac{1}{4}}e^{-0.82\tau} \tag{21}$$

and when $b_0 = 8$ m is approximated by

$$\eta = 0.95\tau^{\frac{1}{4}}e^{-0.80\tau} \tag{22}$$

For strong turbulence, Eq. (17) is used, and the vortex lifespan is independent of the ratio of r_c and b_0.

As shown in Fig. 8, the difference of two curves is very small. In addition, the difference in lifespan between Eqs. (21) and (22) and the modified function of CB,[15] that is, Eq. (20), is also very small. For example, the dimensionless lifespan of the case of $b_0 = 8$ m at $\eta = 0.1$ is only about 2% larger than that of the case of $b_0 = 16$ m, and only about 4% smaller than that of the modified CB function. Note that r_c/b_0 of the case of $b_0 = 8$ m is about 2.5 times larger than that used by CB. This implies that the CB vortex lifespan expression is insensitive to the core radius for a fixed vortex separation.

To determine the lifespan in our simulations, we apply a simple equation formulated by Crow and Murman[30] and CB,[15] that is,

$$B(t) = \frac{b_{\max}(t) - b_{\min}(t)}{b_{\max}(t) + b_{\min}(t)} \tag{23}$$

where $b_{\max}(t)$ and $b_{\min}(t)$ are the maximum and minimum vortex separation distance, respectively, and are estimated in the present study by considering only the y displacement. The normalized amplitude $B(t)$ is zero in the absence of perturbation and becomes unity when the vortices link. Based on the top views of the vortices, the lifespan in the present study is determined as the time when $B(t) = 0.85$.

Dimensionless vortex lifespans from a total of eight simulations for cases of both $b_0 = 16$ and 8 m (see Table 1) are shown in Fig. 8 with those from Sarpkaya and Daly's[7] water tank experiments and Tombach's[5] flight tests. Sarpkaya and Daly's[7] data are the ones for vortex linking or core bursting among the entire data, and not more than 10% of the linking or bursting data set are due to bursting (personal communication with Sarpkaya, 1997). Figure 8 reveals clearly that stronger ambient turbulence enhances the demise of the vortices. The lifespan from our LES is about 40% larger on average than the theoretical value of CB.[15] Despite large difference in *Re* between the LES and the water tank experiment, the LES results agree surprisingly well with Sarpkaya and Daly's data[7] of which lower bound appears to be the theoretical curve of CB.[15] Although not shown in Fig. 8, Liu's[8] data also indicate that the theoretical curve underpredicts the lifespans, especially when the lifespans only due to vortex linking are considered. DNS results of Spalart and Wray[10] also show that the CB[15] curve underestimates the average lifespans of the simulations (about 20%). This agreement between numerical simulations and laboratory experiments is encouraging because

wind shear and stratification are absent in these studies, and thus, only ambient turbulence effects are taken into account. The average lifespan in Tombach's[5] data (Fig. 8) appears to agree roughly with the CB[15] curve, whereas some other flight tests, for example, see CB's Fig. 8, display larger lifespans compared with the theoretical CB curve, which is consistent with our results. Because atmospheric observations of the lifespans are influenced by various sources such as nonhomogeneous atmospheric turbulence, wind shear, and stratification, however, it is difficult to differentiate only the ambient turbulence effect on the vortex lifespan from the others.

On the other hand, the CB[15] curve for weak turbulence is basically obtained using the turbulence strength of the scales of eddies comparable to the MAW that is assumed to reside in the inertial subrange, as mentioned before. Because in the case of $b_0 = 16$ m those excitatory eddies are not within the inertial subrange due to the limited domain size and their strength is much weaker than the turbulence strength if these eddies are within the inertial subrange (Fig. 2), one may anticipate that the lifespan would become larger. However, the lifespans for the case of $b_0 = 8$ m, in which the scales of eddies comparable to the MAW are within the inertial subrange, appear to be nearly the same as those for the case of $b_0 = 16$ m [see Fig. 8; LES results (solid and open circles) for $\eta = 0.0316$ and 0.3506 appear to be almost completely overlapped], implying that the turbulence length scale effects on the vortex lifespan is not important. This is consistent with the results from water tank experiments[7,8] in which the lifespan of the vortices in a turbulent environment are also controlled primarily by the dimensionless turbulence intensity η.

Recently, Sarpkaya[31] has revised the CB[15] model to allow for the variation of the wave length and the integral length scale that are not considered in the original CB analysis. The resulting vortex lifespans in strong and weak turbulence are given by

$$\eta\tau^{\frac{4}{3}} = \tfrac{3}{4} \qquad \text{for} \qquad \tau < 2.5 \tag{24}$$

$$\eta = \tau^{\frac{1}{4}} e^{-0.70\tau} \qquad \text{for} \qquad \tau > 2.5 \tag{25}$$

In Eq. (24), the interaction of strong turbulence with the vortices has been also taken into account. As shown in Fig. 8, our LES data agree very closely with Sarpkaya's[31] modified model rather than CB's.[15]

The normalized amplitude $B(t)$ in Eq. (23) is plotted with time to see the growth of the amplitude during the instability development in quantitative form. A plot of $B(t)$ in semilogarithmic coordinates will display the exponential growth of the instability as a straight line. Figure 9 shows the growth of the amplitude for the cases of $b_0 = 16$ and 8 m. It reveals that the growth is significantly reduced in the middle range of dimensionless time from the fast growth at earlier times. The simulation with larger integral length scale of turbulence, that is, the case of $b_0 = 8$ m, shows faster growth of amplitude in the middle range of dimensionless time than the case with smaller integral length scale, that is, the case of $b_0 = 16$ m, but in later stages the two curves tend to converge, producing nearly the same lifespan. A plot of $B(t)$ from an atmospheric observation by CB displays exponential growth from 30 to about 90 s (see Fig. 3 in Ref. 15), but they did not plot $B(t)$ at earlier times, that is, from 0 to about 30 s, when the growth of amplitude may be much faster than that after 30 s (Fig. 9).

To estimate the magnitude of scatter in the vortex lifespan due to the statistical fluctuations of turbulence, the vortices were injected at different times with about one eddy turnover time interval but still in a statistically steady-state turbulence field. Because the external forcing requires a significant computational effort and has been shown to have a negligible effect on the vortex evolution, it is deactivated after the vortices are injected. The results combined with the lifespans from our LES of Fig. 8 are shown in Fig. 10. The maximum deviations of the simulation results are about 7, 14, and 20% of their averages for $\eta = 0.0316$, 0.1753, and 0.3506, respectively. This increasing scatter with increasing η is consistent with Spalart and Wray's[10] DNS result in which the standard deviation of the simulation results increased to about 20% of the mean for small η and to about 40% of the mean for large η showing much larger scatter in lifespans compared with our LES results. There appears to be a possibility that the scatter in vortex lifespans decreases with

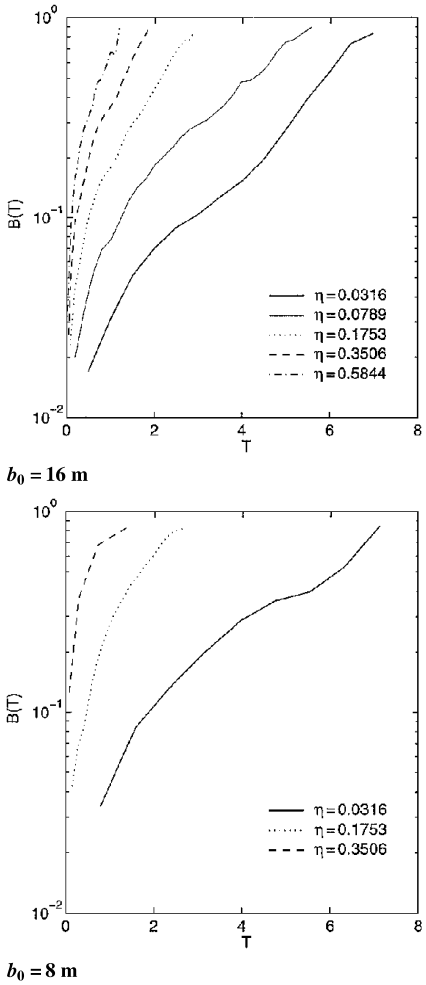

Fig. 9 Amplitude evolution of the instability with varying η for the cases.

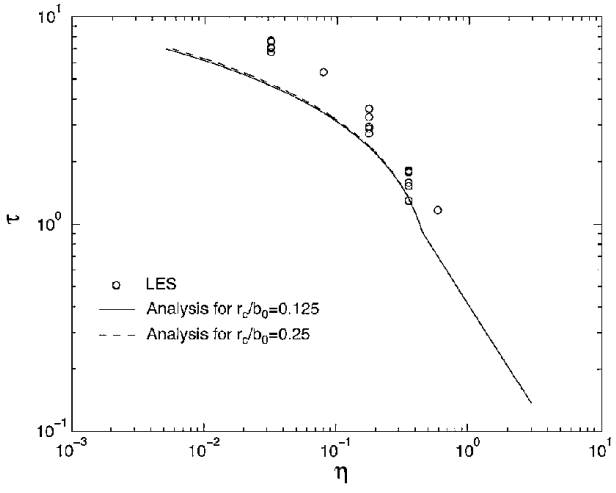

Fig. 10 Dimensionless vortex lifespans from numerical simulations; more lifespans for the case of $b_0 = 8$ m are obtained by injecting the vortices at varying time in a statistically steady-state turbulence with external forcing deactivated.

increasing Reynolds number. For example, the scatter of lifespans in laboratory experiments[7,8] appears to be somewhat larger than that in our simulations (Figs. 8 and 10), although Reynolds numbers in laboratory experiments are much lower than what is possible in the atmosphere. In addition, the Reynolds number in Spalart and Wray's DNS study[10] (about 1.7×10^3–9×10^3) is an order of magnitude less than that in the water tank experiments of Sarpkaya and Daly[7] (about 2.2×10^4–6.6×10^4), whereas the scatter of lifespans

in the DNS results is much larger than that in water tank experiments. However, a formal conclusion for this trend in the scatter of lifespans can be reached only by varying the Reynolds number over several DNSs. On the other hand, the larger scatter of lifespans in flight tests (Fig. 8, about a factor of 3 for fixed η) may result from other factors such as stratification, wind shear, and inhomogeneous atmospheric turbulence.

IV. Conclusions

The effects of ambient atmospheric turbulence on aircraft wake vortices have been studied using a validated LES model. Our results reveal that the MAW of the Crow instability[3] and the lifetime of wake vortices are significantly influenced by ambient atmospheric turbulence. The following conclusions can be drawn from the results of numerical simulations.

1) The Crow instability[3] develops clearly at most atmospheric turbulence levels, but, in strong turbulence, the vortex pair deforms more irregularly due to turbulence advection.

2) The MAW of the instability decreases with increasing dimensionless ambient turbulence level, which are consistent with laboratory experiments[8] and atmospheric observations.[4]

3) Turbulence with smaller integral length scale ($b_0 = 16$ m), in which the theoretical MAW ($8.2b_0$) is not within the inertial subrange, leads to smaller MAW that is less than the theoretical value. On the other hand, turbulence with a larger integral length scale ($b_0 = 8$ m), in which the theoretical MAW ($6.9b_0$) is within the inertial subrange, leads to larger MAW.

4) Consistent with results of laboratory experiments,[7,8] vortex lifespan is primarily controlled by dimensionless turbulence intensity η and decreases with increasing η, whereas the integral scale of turbulence is of minor importance to vortex lifespan.

5) The lifespan is estimated to be about 40% larger than that in the theoretical prediction by CB.[15] However, this larger lifespan agrees very well with the data from laboratory experiments and Sarpkaya's[31] modification to CB's theory.[15]

6) The maximum deviation in lifespan from the average value due to ambient turbulence alone is about 7% of the mean for small η and about 20% of the mean for large η, showing much less scatter in lifespan compared with flight tests[5] and DNS.[10] There appears to be a possibility that the scatter in vortex lifespans decreases with increasing Reynolds number, although a formal conclusion can be reached only by varying Reynolds number over several DNSs. On the other hand, larger scatter of lifespans in flight tests may result from other factors, such as stratification, wind shear, and inhomogeneous ambient turbulence.

Acknowledgments

This work was supported by NASA's Terminal Area Productivity program under Contract NAS 1-18925 (Cooperative Agreement NCC-1-188). Numerical simulations were carried out on NASA's Cray C90 and J90 and North Carolina Supercomputing Center's Cray T916. The authors would like to thank T. Sarpkaya for providing his experimental data and Tombach's flight test data, as well as for his helpful comments. Discussions with C.-T. Kao, D. S. Decroix, and S. Shen are also highly appreciated. Some results from the simulations considered here were originally presented at the NASA First Wake Vortex Dynamic Spacing Workshop, 13–15 May 1997.

References

[1]Hinton, D. A., "Aircraft Vortex Spacing System (AVOSS) Conceptual Design," NASA TM-110184, 1995.

[2]Perry, R. B., Hinton, D. A., and Stuever, R. A., "NASA Wake Vortex Research for Aircraft Spacing," AIAA Paper 97-0057, Jan. 1997.

[3]Crow, S. C., "Stability Theory for a Pair of Trailing Vortices," *AIAA Journal*, Vol. 8, No. 12, 1970, pp. 2172–2179.

[4]Chevalier, H., "Flight Test Studies of the Formation and Dissipation of Trailing Vortices," *Journal of Aircraft*, Vol. 10, No. 1, 1973, pp. 14–18.

[5]Tombach, I., "Observations of Atmospheric Effects on Vortex Wake Behavior," *Journal of Aircraft*, Vol. 10, No. 11, 1973, pp. 641–647.

[6]Sarpkaya, T., "Trailing Vortices in Homogeneous and Density-Stratified Media," *Journal of Fluid Mechanics*, Vol. 136, 1983, pp. 85–109.

[7]Sarpkaya, T., and Daly, J. J., "Effect of Ambient Turbulence on Trailing Vortices," *Journal of Aircraft*, Vol. 24, No. 6, 1987, pp. 399–404.

[8]Liu, H.-T., "Effects of Ambient Turbulence on the Decay of a Trailing Vortex Wake," *Journal of Aircraft*, Vol. 29, No. 2, 1992, pp. 255–263.

[9]Lewellen, D. C., and Lewellen, W. S., "Large-Eddy Simulations of the Vortex-Pair Breakup in Aircraft Wakes," *AIAA Journal*, Vol. 34, No. 11, 1996, pp. 2337–2345.

[10]Spalart, P. R., and Wray, A. A., "Initiation of the Crow Instability by Atmospheric Turbulence," *78th AGARD-FDP Symposium on the Characterization and Modification of Wakes from Lifting Vehicles in Fluids*, May 1996, pp. 18:1–18.

[11]Bisgood, P. L., "Some Observations of Condensation Trails," Royal Aeronautical Establishment, TM, FS-530, 1980.

[12]Donaldson, C. duP., and Bilanin, A. J., "Vortex Wakes of Conventional Aircraft," AGARDograph 204, May 1975.

[13]Greene, G. C., "An Approximate Model of Vortex Decay in the Atmosphere," *Journal of Aircraft*, Vol. 23, No. 7, 1986, pp. 566–573.

[14]Han, J., Lin, Y.-L., Schowalter, D. G., Arya, S. P., and Proctor, F. H., "Large-Eddy Simulation of Aircraft Wake Vortices: Atmospheric Turbulence Effects," *12th Symposium on Boundary Layers and Turbulence*, 1997, pp. 237–238.

[15]Crow, S. C., and Bate, E. R., "Lifespan of Trailing Vortices on a Turbulent Atmosphere," *Journal of Aircraft*, Vol. 13, No. 7, 1976, pp. 476–482.

[16]Moeng, C.-H., "A Large Eddy Simulation Model for the Study of Planetary Boundary Layer Turbulence," *Journal of Atmospheric Sciences*, Vol. 41, No. 13, 1984, pp. 2052–2062.

[17]Mason, P. J., "Large Eddy Simulation of the Convective Boundary Layer," *Journal of Atmospheric Sciences*, Vol. 46, No. 11, 1989, pp. 1492–1516.

[18]Schmidt, H., and Schumann, U., "Coherent Structure of the Convective Boundary Layer Derived from Large Eddy Simulations," *Journal of Fluid Mechanics*, Vol. 200, 1989, pp. 212–248.

[19]Proctor, F. H., "The Terminal Area Simulations System, Volume 1: Theoretical Formulation," NASA CR 4046, DOT/FAA/PM-86/50, 1, 1987.

[20]Proctor, F. H., "Numerical Simulation of Wake Vortices Measured During the Idaho Fall and Memphis Field Programs," *Proceedings of the AIAA 14th Applied Aerodynamics Conference*, Pt. 2, AIAA, Reston, VA, 1996, pp. 943–960.

[21]Proctor, F. H., Hinton, D. A., Han, J., Schowalter, D. G., and Lin, Y.-L., "Two Dimensional Wake Vortex Simulations in the Atmosphere: Preliminary Sensitivity Studies," AIAA Paper 97-0056, Jan. 1997.

[22]Klemp, J. B., and Wilhelmson, R. B., "The Simulation of Three-Dimensional Convective Storm Dynamics," *Journal of Atmospheric Sciences*, Vol. 35, No. 6, 1978, pp. 1070–1096.

[23]Switzer, G. F., "Validation Tests of TASS for Application to 3-D Vortex Simulation," NASA CR 4756, 1996.

[24]Rosenhead, L., "The Spread of Vorticity in the Wake behind a Cylinder," *Proceedings of the Royal Society of London, Series A: Mathematical and Physical Sciences*, Vol. A127, 1930, pp. 590–612.

[25]Burnham, D. C., and Hallock, J. N., "Chicago Monostatic Acoustic Vortex Sensing System, Vol. 4: Wake Vortex Decay," National Technical Information Service, Springfield, VA, 1982.

[26]Vincent, A., and Meneguzzi, M., "The Spatial Structure and Statistical Properties of Homogeneous Turbulence," *Journal of Fluid Mechanics*, Vol. 225, 1991, pp. 1–20.

[27]Champagne, F. H., Friehe, C. A., LaRue, J. C., and Wyngaard, J. C., "Flux Measurements, Flux Estimation Techniques, and Fine-Scale Turbulence Measurements in the Unstable Surface Layer Over Land," *Journal of Atmospheric Sciences*, Vol. 34, No. 3, 1977, pp. 515–530.

[28]Jeong, J., and Hussain, F., "On the Identification of a Vortex," *Journal of Fluid Mechanics*, Vol. 285, 1995, pp. 69–94.

[29]Corjon, A., Risso, F., Stoessel, A., and Poinsot, T., "Three-Dimensional Direct Numerical Simulations of Wake Vortices: Atmospheric Turbulence Effects and Rebound with Crosswind," *78th AGARD-FDP Symposium on the Characterization and Modification of Wakes from Lifting Vehicles in Fluids*, 1996, pp. 28:1–21.

[30]Crow, S. C., and Murman, E. M., "Trailing-Vortex Experiments at Moses Lake," Boeing Scientific Research Lab., Communication 009, The Boeing Co., Seattle, WA, Feb. 1970.

[31]Sarpkaya, T., "Decay of Wake Vortices of Large Aircraft," *AIAA Journal*, Vol. 36, No. 9, 1998, pp. 1671–1679.

S. K. Aggarwal
Associate Editor